Supporting information

Synergistic Optimization of Minimal Antisolvent Processing and Dopant-Free HTMs for High-Efficiency Perovskite Solar Cells

Eun Seo Oh[a], Jinyoung Kim[a], Yuya Ohkura[b], Toshiaki Ito[b], Yuichiro Hayashi[b], Hideaki Takahashi[b], Hiroshi Sato[b], Naoyuki Shibayama[c], Tsutomu Miyasaka[c], Simon MoonGeun Jung [a,d] *, Gyu Min Kim[a]*

[a]Department of Chemical Engineering, Research Center of Chemical Technology, Hankyong National University, Anseong 17579, Gyeonggi-do, Republic of Korea

[b]Hodogaya Chemical Co., Ltd.45 Miyukigaoka, Tsukuba, Ibaraki 305–0841, Japan

[c]Graduate School of Engineering, Toin University of Yokohama, 1614 Kurogane-cho, Aoba, Yokohama, Kanagawa 225-8503, Japan

[d]Research Institute of Carbon Neutral Convergence Technology, Hankyong National University, Anseong 17579, Korea

*Correspondence

E-mail: gyumin@hknu.ac.kr, mgjung@hknu.ac.kr

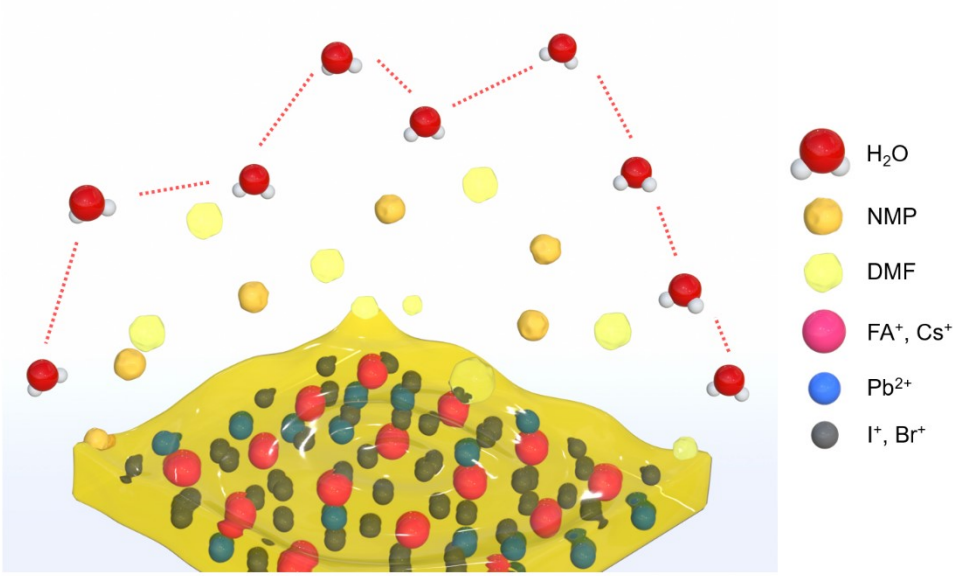

Figure S1 Mechanism of humidity and precursor evaporation interaction

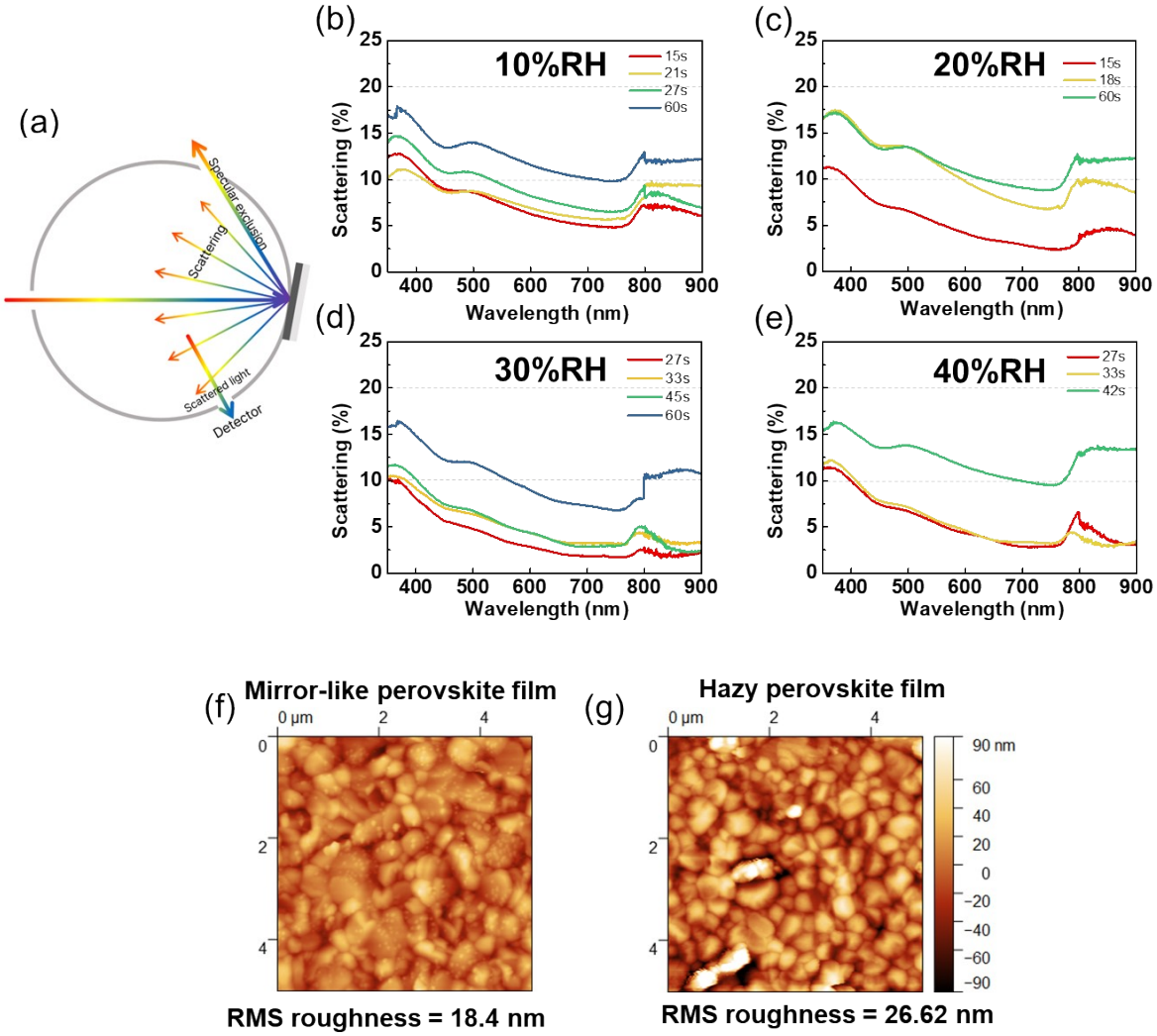

Figure S2. (a) Illustration of scattering measurement. Perovskite film scattering at (b) 30%, (c) 10%, (d) 20%, and (e) 40%. (Right legend indicates anti-solvent dripping time). AFM image of (f) mirror-like perovskite film, (g) and hazy perovskite film.

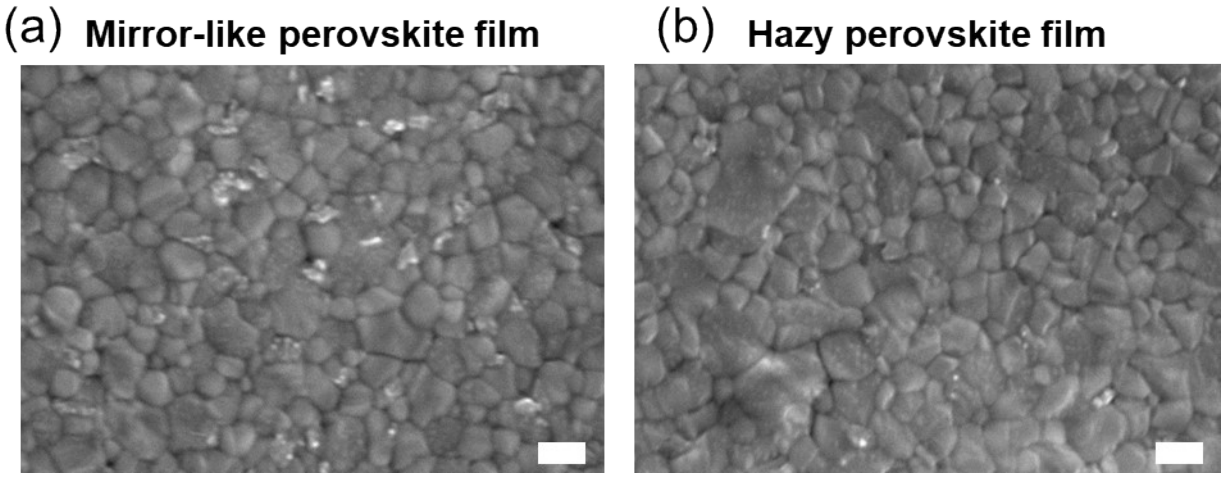

Figure S3. (a) SEM image of mirror-like perovskite film, (b) and hazy perovskite film. (scale bar : 5μm)

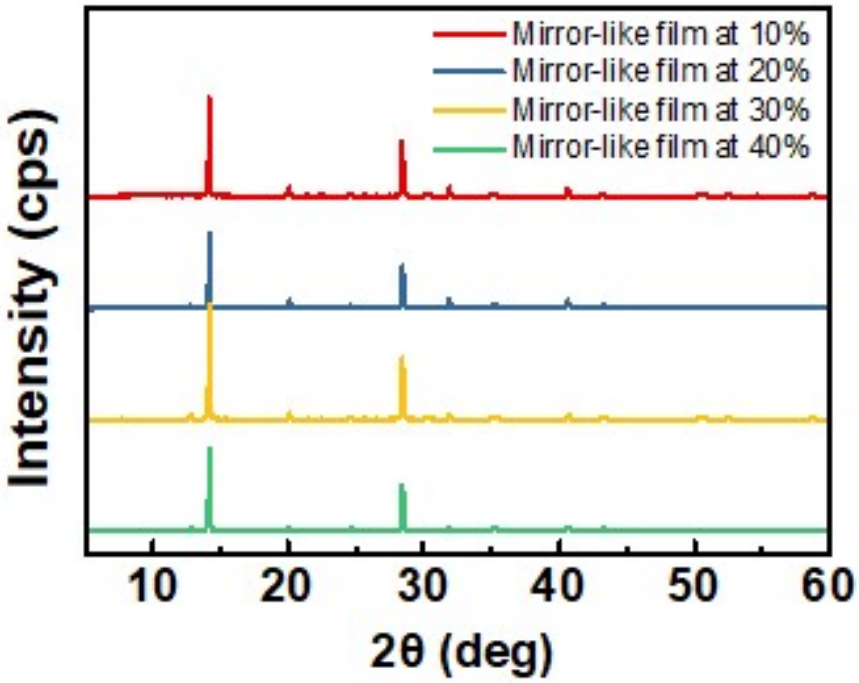

Figure S4. XRD patterns of mirror-like surface perovskite film manufactured at each humidity.

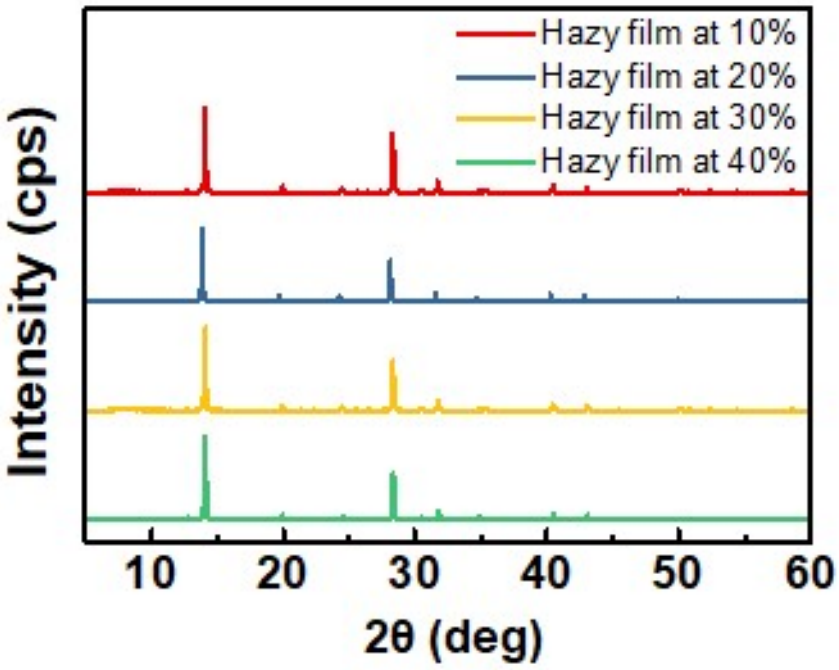

Figure S5. XRD patterns of hazy perovskite film manufactured at each humidity.

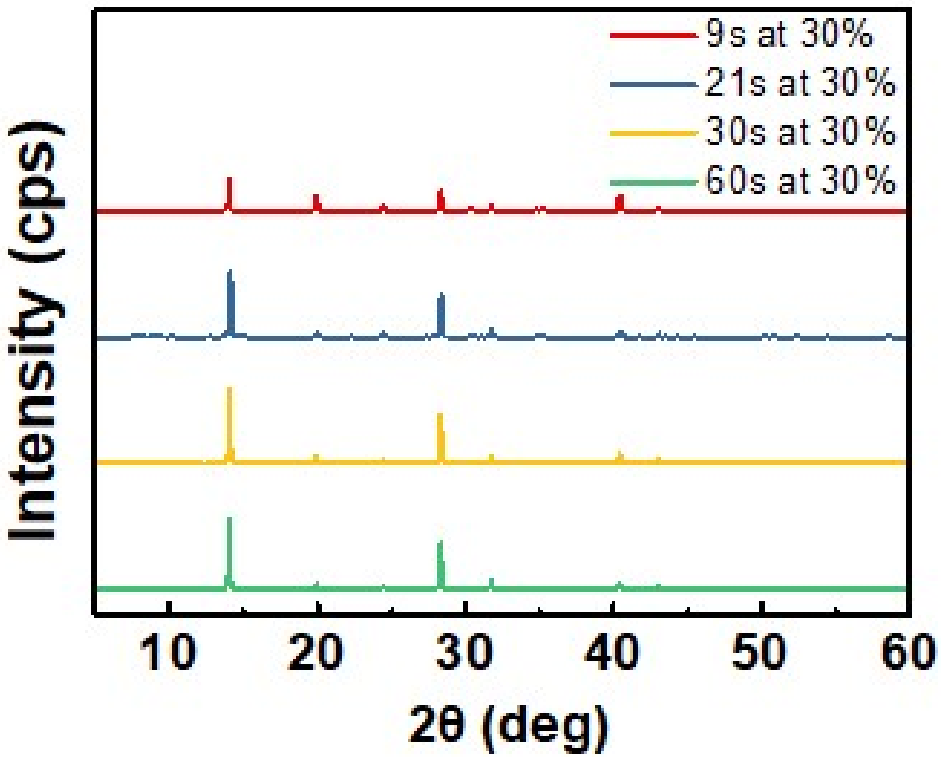

Figure S6. XRD patterns of perovskite film manufactured at each dripping timing of anti-solvent at 30%.

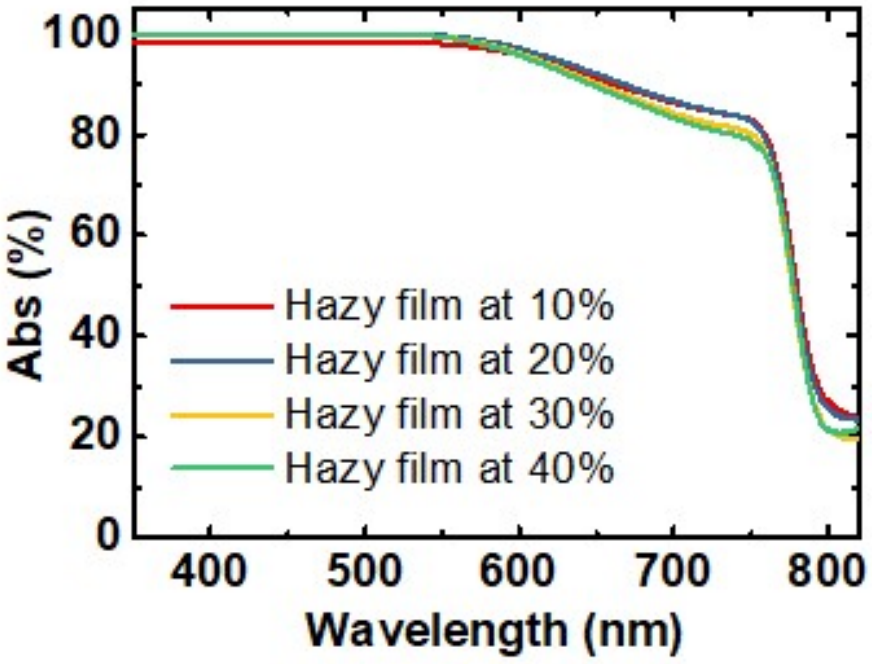

Figure S7. UV-vis absorbance according to humidity on hazy surfaces

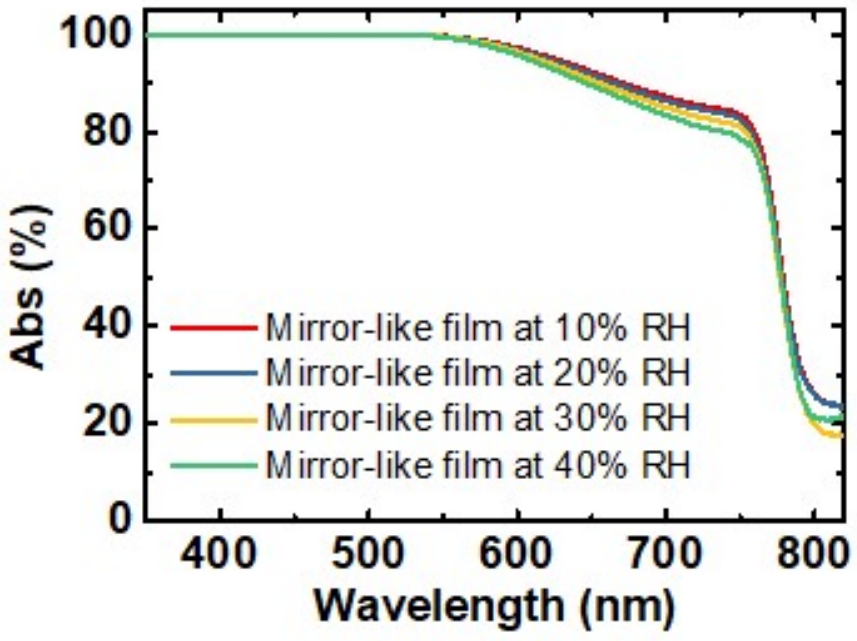

Figure S8. UV-vis absorbance according to humidity on mirror-like surfaces.

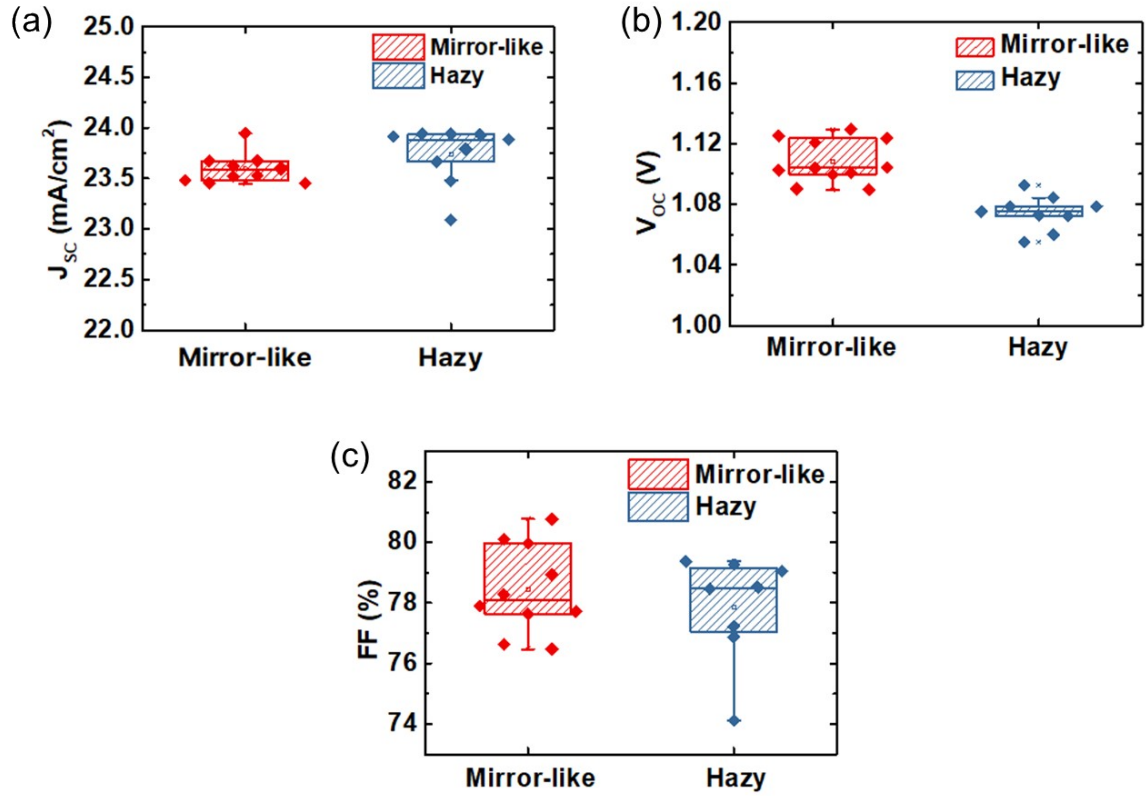

Figure S9. Box plot of (a) J_{SC}, (b) V_{OC}, (c) fill factor (FF) according to perovskite surface.

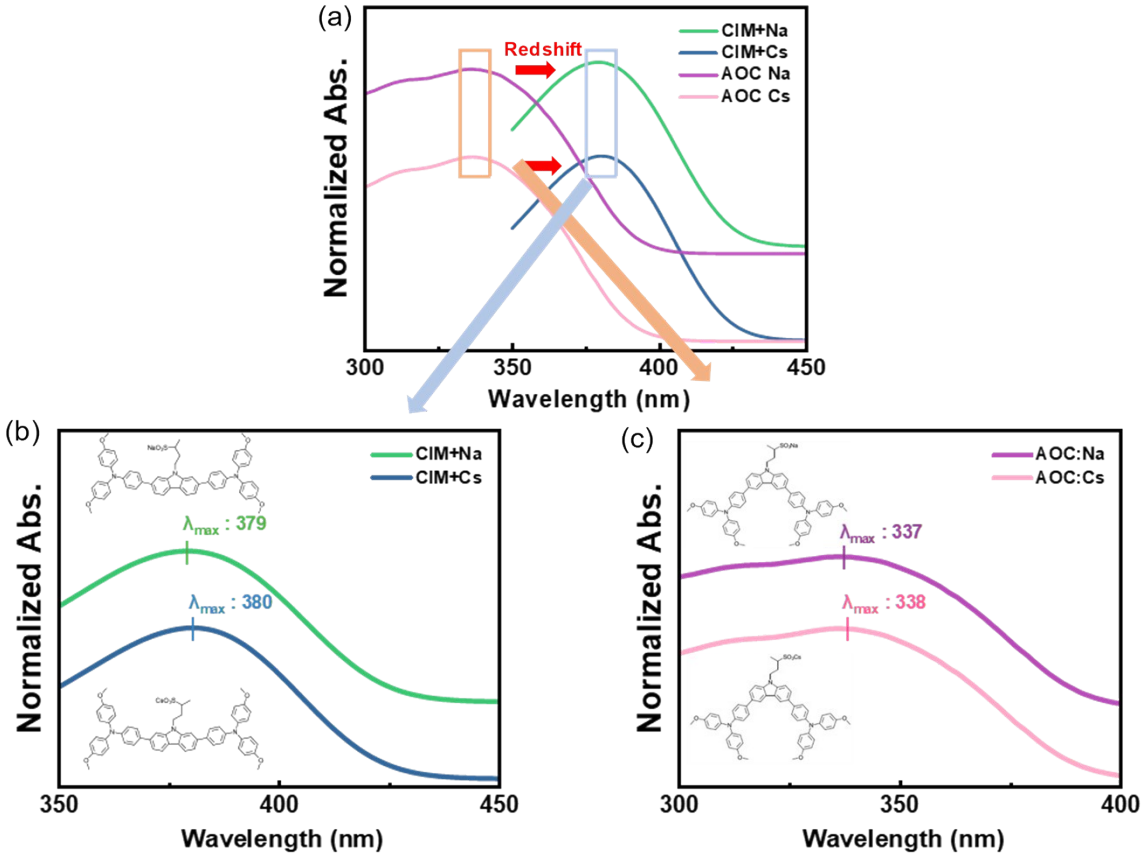

Figure S10. UV–vis absorption(Abs) spectra of HTMs from previous study (AOC series) and CIM series. (a) Total Abs spectra of HTM's, (b) CIM+Na and CIM+Cs, and (c) AOC:Na and AOC:Cs in solution.

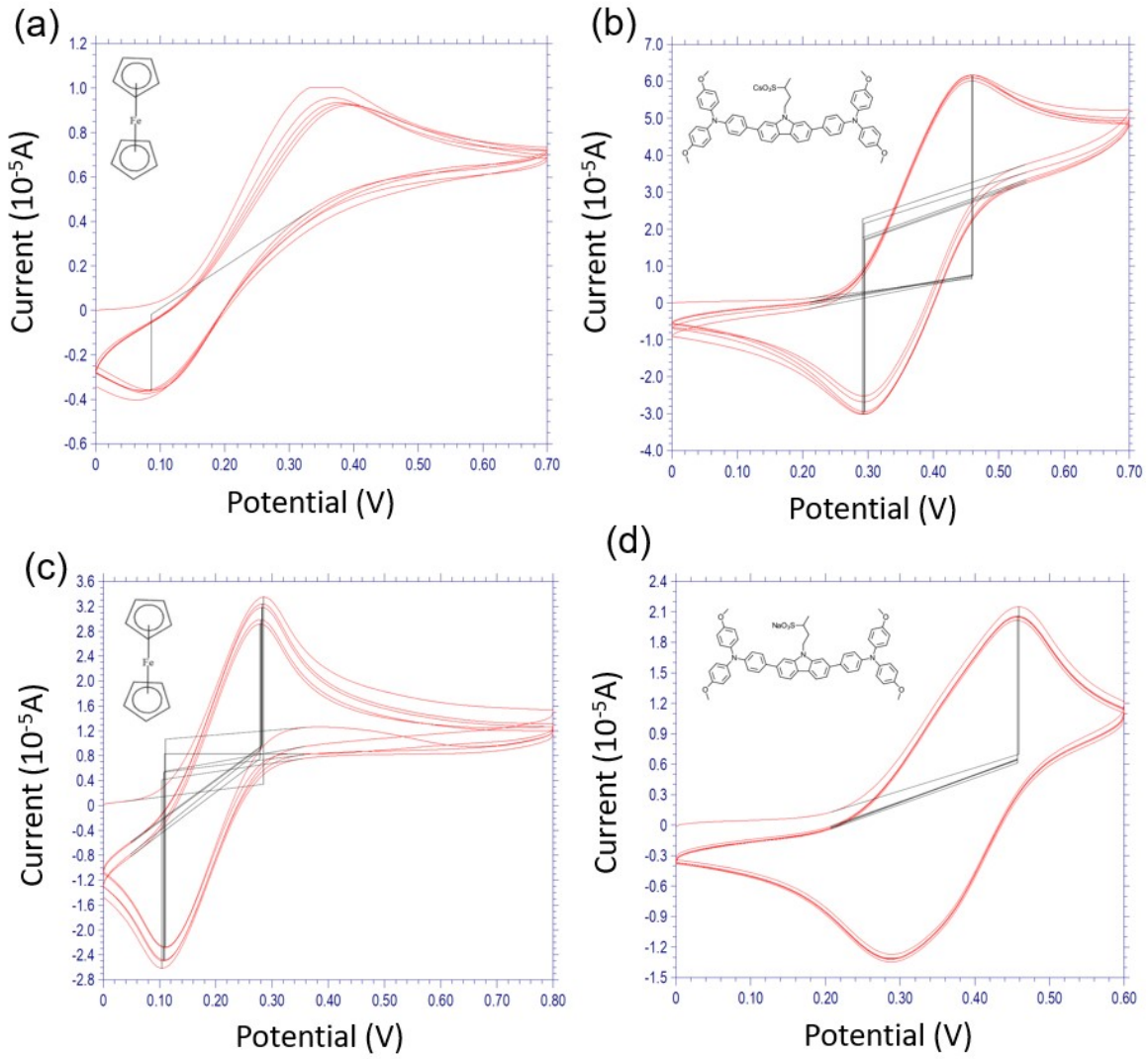

Figure S11. Cyclic voltammetry (CV) curves of (a) ferrocene (standard for CIM+Cs measurements), (b) CIM+Cs, (c) ferrocene (standard for CIM+Na measurements), and (d) CIM+Na.

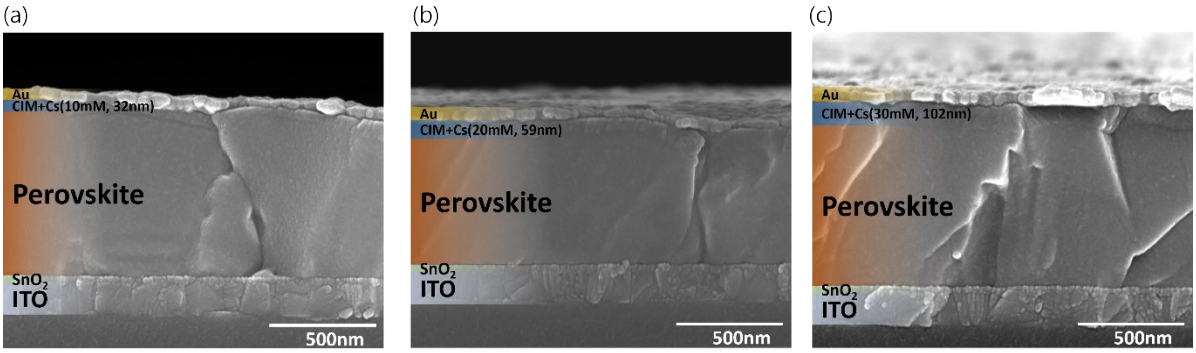

Figure S12. Cross-section SEM images of (a) 10mM, (b) 20mM, and (c) 30mM CIM+Cs layers. Each layer's thickness is 32nm, 59nm and 102nm.

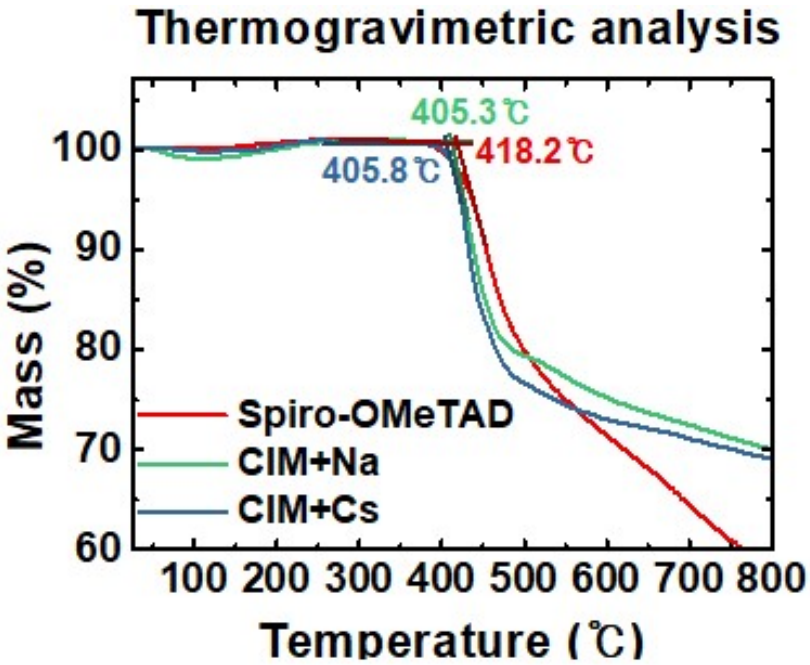

Figure S13. TGA analysis of Spiro-OMeTAD, CIM+Na, and CIM+Cs from 25°C to 800°C.

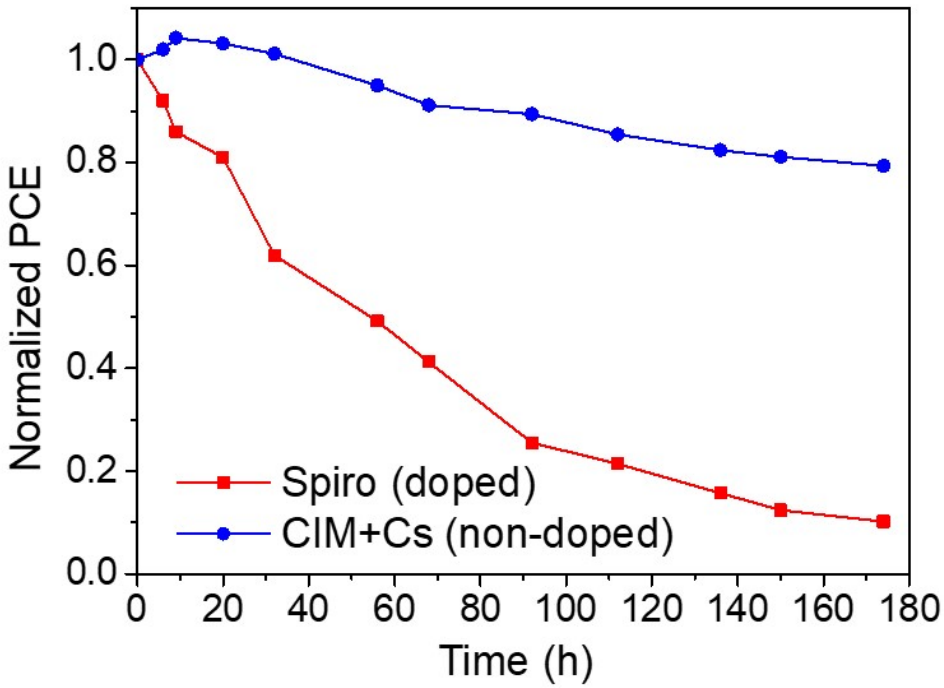

Figure S14. Normalized PCEs of PSCs based on doped Spiro and dopant-free CIM+Cs as HTLs, measured under thermal aging conditions (60 °C, RH < 1%) in a dry ambient atmosphere.

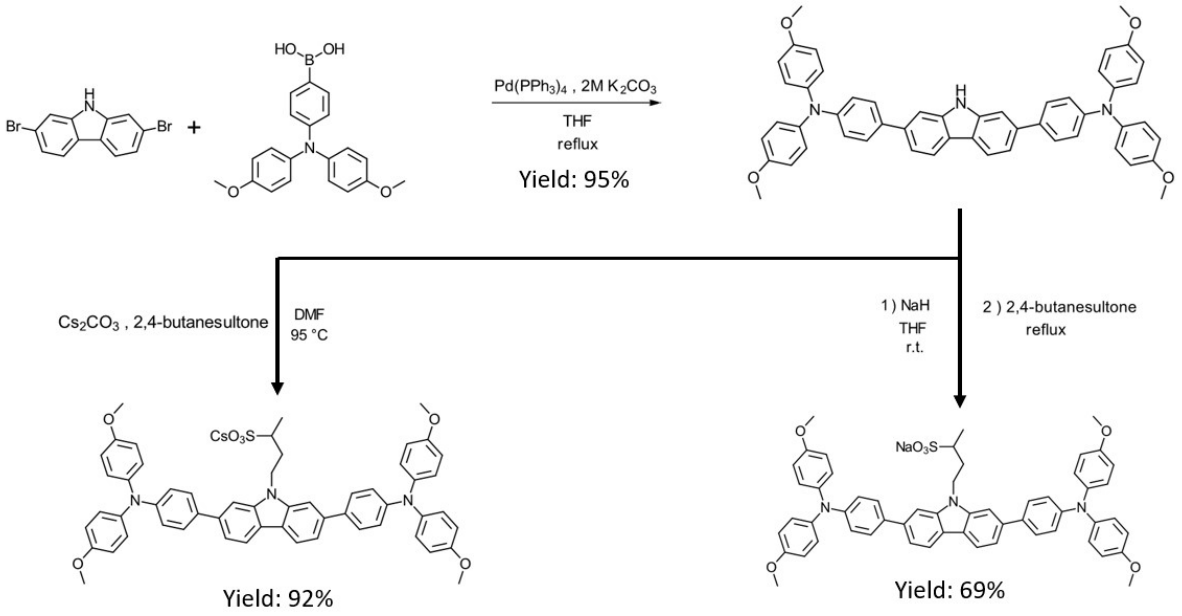

Figure S15. Synthetic routes and yields for the preparation of CIM+Na and CIM+Cs

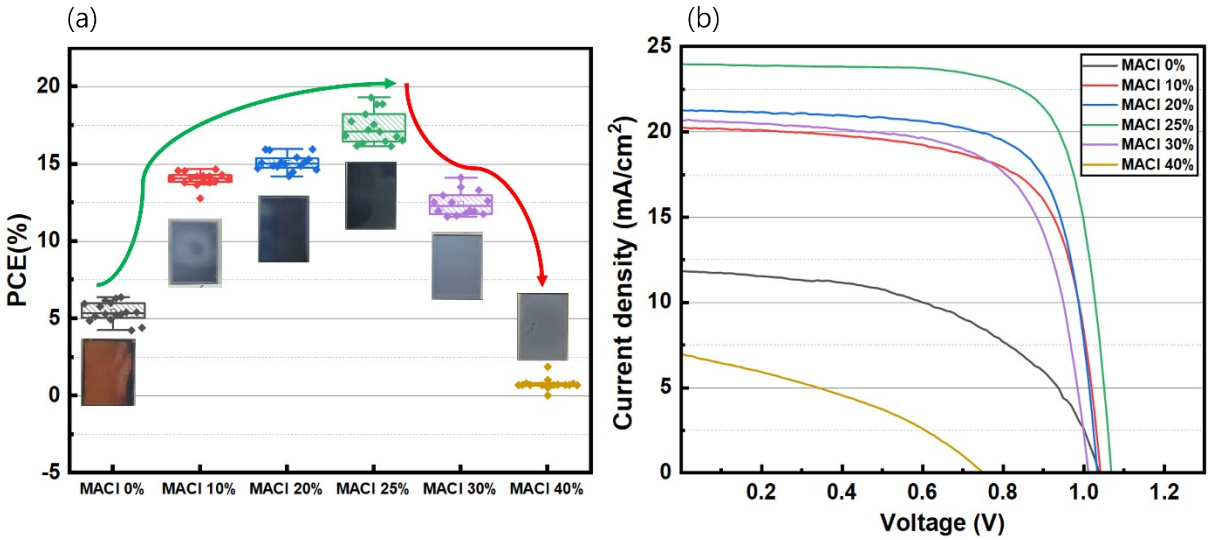

Figure S16. Performance of devices depending on MACl concentration, which is in range of 0, 10, 20, 25, 30, and 40mol%. (a) is statistics of devices and (b) is the best *J*-V curve of each condition. The specific values are displayed in Table S2.

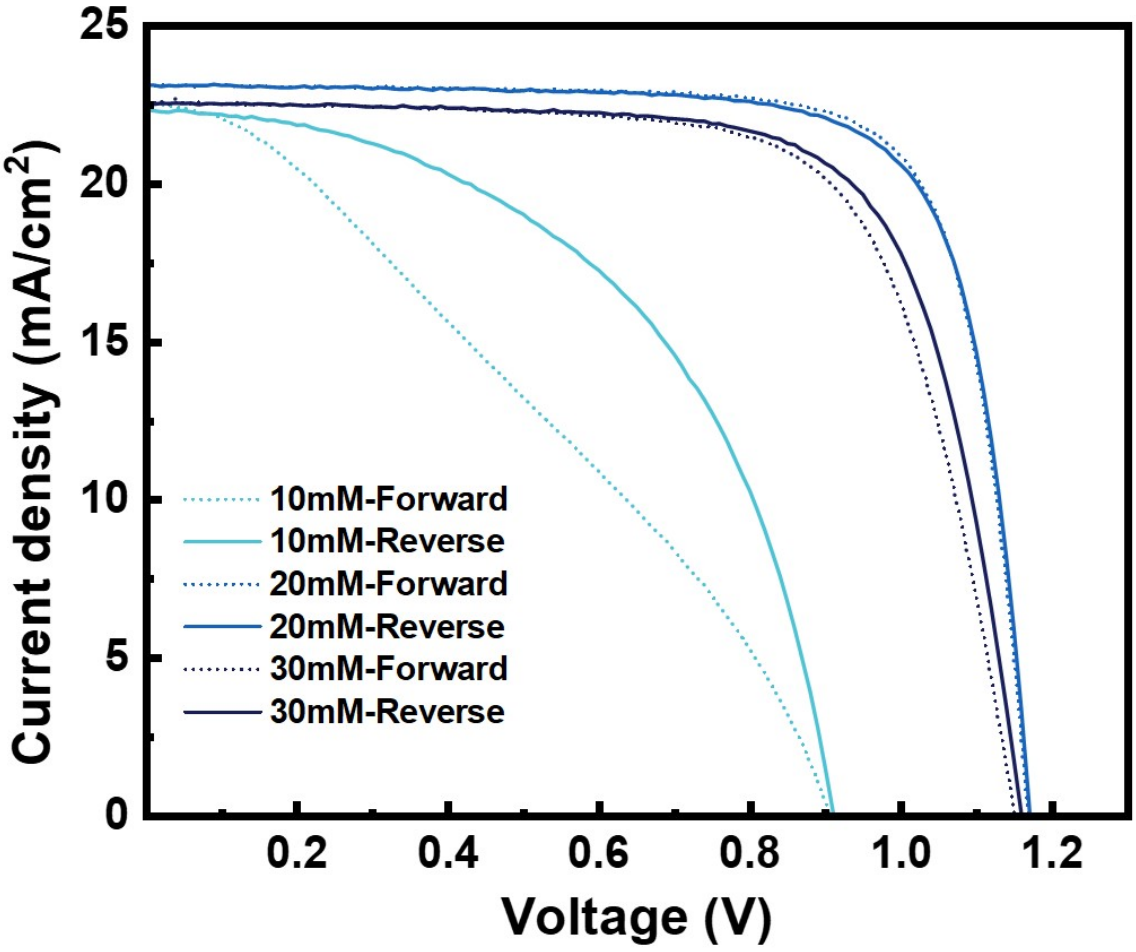

Figure S17. *J–V* curves (forward and reverse scan) of PSCs fabricated with dopant-free CIM+Cs HTL at varying concentrations (10 mM, 20 mM, and 30 mM).

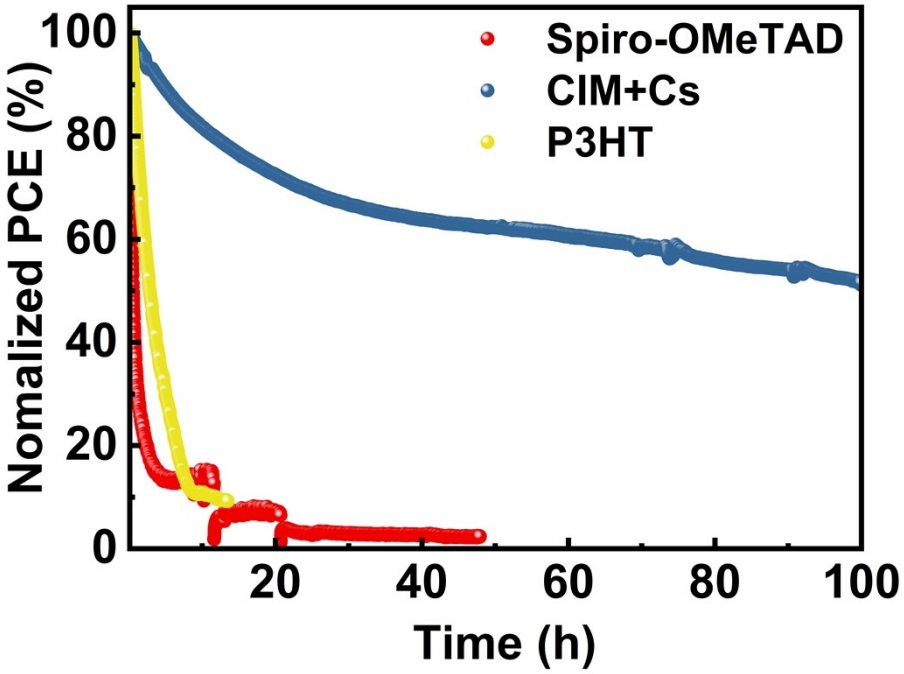

Figure S18. Steady-state power output (SPO) stability of devices employing doped Spiro-OMeTAD, CIM+Cs, and dopant-free P3HT.

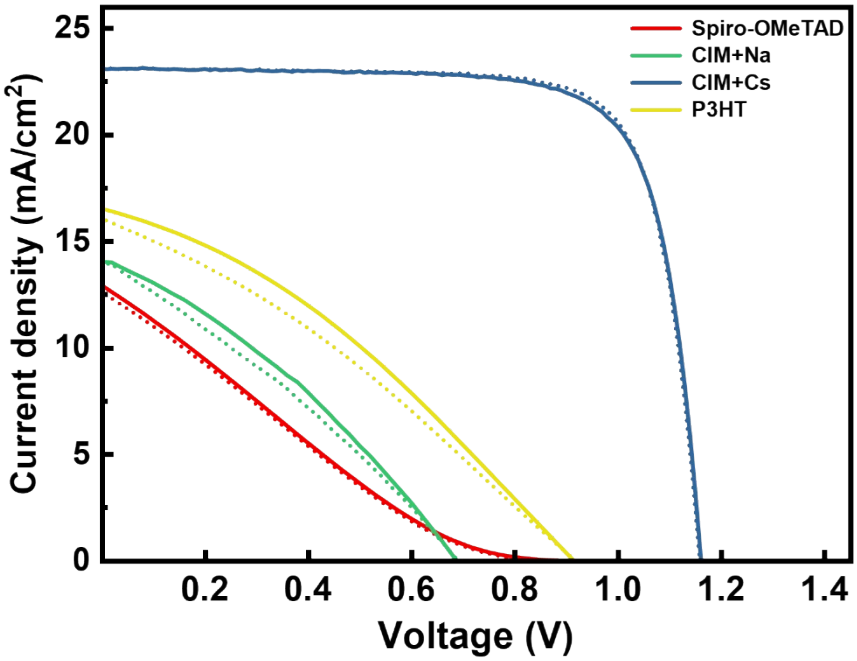

Figure S19. J-V curves of devices employing dopant-free hole transport materials: CIM-Na, CIM-Cs, P3HT, and Spiro-OMeTAD. Solid line is forward scan and dash line is reverse scan. The specific value is denoted in Table S2.

Table S1. The result of cyclic voltammetry (CV) of CIM+Na and CIM+Cs.

Material	CV oxidation peak (V, vs Ag/AgCl)	Ferrocene E_p (V)	GSOP (V vs Fc/FC^+)	HOMO (eV)	Eg (eV)	LUMO (ev)
CIM+Na	0.459	0.285	0.174V	-4.97	2.92	-2.05
CIM+Cs	0.459	0.330	0.129V	-4.93	2.91	-2.02

Table S2. Parameters from the best *J*-V curves of each MACl concentration.

MACl (mol%)	J_{SC} (mA/cm^2)	V_{OC} (V)	FF	PCE (%)
0	11.85	1.04	0.52	6.38
10	20.26	1.04	0.70	14.65
20	21.29	1.03	0.73	15.96
25	23.98	1.07	0.75	19.30
30	20.67	1.01	0.68	14.12
40	6.98	0.76	0.36	1.88

Table S3. Parameters from the best *J*-V curves of dopant free HTM.

HTM (Dopant free)	J_{SC} (mA/cm^2)	V_{OC} (V)	FF	PCE (%)
Spiro-OMeTAD – Forward	12.75	0.86	0.20	2.23
Spiro-OMeTAD – Reverse	12.88	0.88	0.20	2.28
CIM+Na – Forward	14.24	0.70	0.29	2.90
CIM+Na – Reverse	14.20	0.70	0.32	3.18
CIM+Cs – Forward	23.11	1.17	0.77	20.9
CIM+Cs – Reverse	23.11	1.17	0.76	20.6
P3HT – Forward	16.13	0.92	0.31	4.55
P3HT – Reverse	16.50	0.91	0.33	5.04

Table S4. λmax and band gap value of HTM's including AOC series.

Hole transport materials (HTL)	λ_{max} [nm]	E_g [eV]	CBM [eV]	VBM [eV]
Spiro-OMeTAD	389	2.97	-1.98	-4.95
CIM+Na	379	2.92	-2.34	-5.26
CIM+Cs	380	2.91	-2.37	-5.28
AOC-Na	337	3.16	-2.00	-5.16
AOC-Cs	338	3.15	-2.05	-5.20